ACS Catalysis

Research Article

pubs.acs.org/acscatalysis

# Pd-Modified Tungsten Carbide for Methanol Electro-oxidation: From Surface Science Studies to Electrochemical Evaluation

Zachary J. Mellinger, Thomas G. Kelly, and Jingguang G. Chen*

Center for Catalytic Science and Technology, Department of Chemical Engineering, University of Delaware, Newark, Delaware 19716, United States

**ABSTRACT:** The current study explores the potential utilization of tungsten monocarbide (WC) and Pd-modified WC as anode electrocatalysts in direct methanol fuel cells (DMFC). Density functional theory (DFT) calculations and ultrahigh vacuum (UHV) studies were performed to determine how the presence of Pd affected the bonding and reaction pathways of methanol on the WC surface. These studies showed that the WC surface was very active toward the O−H bond cleavage to produce a methoxy intermediate, although WC was less active for the C−H bond scission. Adding Pd on WC enhanced the scission of the C−H bonds of methoxy, suggesting a synergistic effect of using Pd-modified WC as electrocatalysts for methanol decomposition. The prediction from UHV studies was verified in electrochemical experiments using cyclic voltammetry (CV) and chronoamperometry (CA) measurements of electro-oxidation of methanol in an alkaline environment.

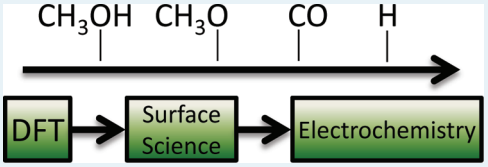


**KEYWORDS:** *methanol electrooxidation, CO tolerance, WC, Pd/WC, electrocatalyst*

## 1. INTRODUCTION

Low-temperature fuel cells have been the subject of extensive investigations as high efficiency power sources. They are especially ideal for portable applications, as they have a relatively high power density while still operating at low temperatures. Hydrogen and alcohols are some of the fuels that have been investigated. In liquid form, methanol[1,2] has higher energy density than hydrogen gas while also integrating well with the existing energy infrastructure. The electro-oxidation of methanol in direct methanol fuel cells[3−5] (DMFC) is currently being investigated by many research groups.

Currently the most promising anode catalysts used in DMFC are Pt and Pt-based alloys.[6,7] Pt has limitations for large scale applications because of its limited abundance and high cost. In comparison, Pd is fifty times more abundant[8] and often shows similar catalytic properties to Pt. Furthermore, Pt is easily poisoned by adsorbed CO that is present in hydrogen produced by steam reforming and also as an intermediate in methanol oxidation.[9,10] Pd-based catalysts have shown increased CO tolerance and a higher methanol oxidation activity in an alkaline environment when compared to Pt catalysts.[11−13]

One way to significantly decrease the precious metal loading in electrocatalysts is to use a support that is electrochemically active and stable. Many supports have been investigated, but a group of supports that have shown promise are transition metal carbides, specifically tungsten monocarbide (WC).[14] One reason that WC has been used as the substrate is its similar bulk electronic properties to Pt-group metals.[15] Furthermore, metal-modified WC electrocatalysts have shown increased CO tolerance.[16,17] The WC support has been postulated to help increase the dispersion of the precious metal.[18] In addition, the WC surface is active toward the dissociation of $H_2O$ to produce surface hydroxyl groups,[19] which are critical for the subsequent oxidation of the CO reaction intermediate in DMFC.

In a recent electrochemical study Lee et al. reported that shape controlled Pd/WC nanoparticles showed improved activity for the electro-oxidation of methanol as compared to standard Pd/C catalysts[20] in an alkaline electrochemical environment. Alkaline environments have shown better kinetics than acid environments for fuel oxidation, especially for Pd based catalysts.[8] Alkaline environments also help reduce oxide formation on the surface. Fundamental studies on well-characterized thin films are needed to further understand the promising electrocatalytic properties of Pd/WC. In the current paper, we utilize a combination of ultrahigh vacuum (UHV) surface science studies and electrochemical evaluation of WC films, both with and without Pd modification, for methanol decomposition and electro-oxidation. Density functional theory (DFT) calculations were also performed to compare the binding energies of methanol and methoxy on WC and Pd-modified surfaces. These results demonstrate that modification of WC with low coverages of Pd increases the activity toward both methanol decomposition in UHV studies and methanol electro-oxidation in electrochemical evaluations.

## 2. EXPERIMENTAL AND THEORETICAL METHODS

**2.1. Calculation Methods.** DFT calculations were performed with the Vienna Ab-initio Simulation Package (VASP).[21−23] The PW91 functional was used for electronic structure calculations, and pseudopotentials were used to

**Special Issue:** Electrocatalysis

**Received:** November 29, 2011
**Revised:** February 14, 2012
**Published:** March 16, 2012

   dx.doi.org/10.1021/cs200620x | *ACS Catal.* 2012, 2, 751−758

represent the core electrons. The WC surfaces were represented by a 3 × 3 hcp(0001) unit cell, as described previously[24] and shown in Figure 1. The k-point mesh was 3 × 3 × 1. The energy cutoff was 396 eV, and calculations were spin-polarized. Three layers of WC were used in the calculation, with the bottom two layers being fixed while the top layer was allowed to relax during calculations. For the Pd/WC surface, one monolayer Pd was placed epitaxially on the WC slab. For comparison, similar calculations were also performed on a Pd(111) surface. For each adsorbate, different binding sites were calculated to determine the most stable bonding configuration. The binding energies of methanol and methoxy were calculated by subtracting the clean slab and gas-phase adsorbate energies from the adsorbate-slab supercell.

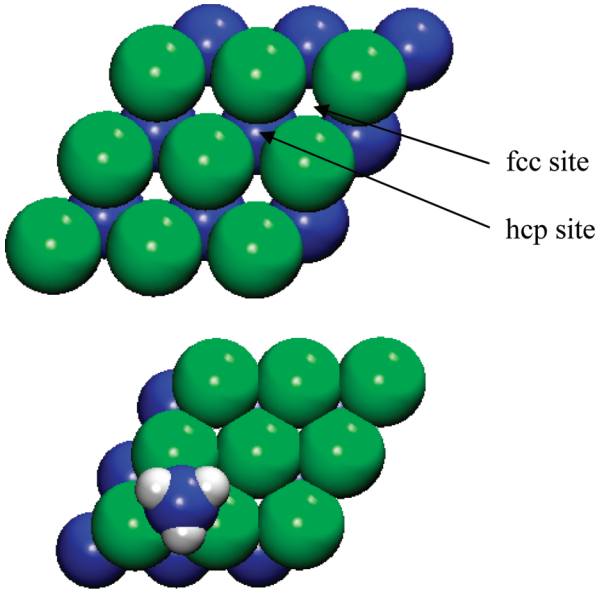


**Figure 1.** Top view of the WC(0001) slab with and without methoxy bound in the fcc position used in DFT calculations. Tungsten is represented as green, carbon is represented as blue, and hydrogen is represented as white.

**2.2. Experimental Methods.** *2.2.1. UHV Studies.* The polycrystalline tungsten foil surface was cleaned by $Ne^+$ bombardment at 300 K followed by annealing to 1100 K. The clean W foil was subsequently sputtered with $C_2H_4$(g) at 300 K, followed by annealing in vacuum to 1200 K as described in detail previously.[25] This procedure was repeated until a stoichiometric WC surface was verified by Auger electron spectroscopy (AES) measurements. The WC stoichiometry was determined based on the intensity ratio of the W(MNN 182 eV)/C(KLL 275 eV) peaks with normalization by AES sensitivity factors.[26] The stoichiometry and phase purity of the WC film have been studied by Weigert et al. using X-ray photoelectron spectroscopy (XPS) and glancing incidence X-ray diffraction (GIXRD).[27] The C 1s peak position was characteristic of carbidic carbon. The atomic W/C ratio, derived from the XPS W 4f and C 1s peak areas and the corresponding sensitivity factors, was determined to be 1.0, indicating that the surface stoichiometry was WC within the detection limit of XPS. Furthermore, the phase purity of the WC film was confirmed in the GIXRD pattern.

The Pd-modified WC surfaces were prepared by depositing Pd on the WC surface at 300 K using a deposition source of Pd wire (99.99% purity) wrapped around a resistively heated tungsten filament. The Pd coverage was estimated by using the AES intensity ratio of the W(MNN 182 eV) and Pd(MNN 333 eV) peaks after deposition.[28] The ratio for the different overlayer coverages of Pd was calculated from the equation provided by Cumpson and Seah.[29]

The UHV chamber used for the temperature programmed desorption (TPD) measurements (base pressure 1 × $10^{-10}$ Torr) was equipped with AES for surface characterization and a quadrupole mass spectrometer (UTI 100C) for TPD measurements. The W foil was spot-welded to two tantalum posts that served as thermal and electrical conductors for liquid-nitrogen cooling and resistive heating. Methanol and CO were dosed at 100 K by backfilling the UHV system. TPD measurements were performed on WC, Pd/WC, and Pd(111) surfaces. TPD quantification was calculated using procedures described previously.[30]

The surface adsorbates and intermediates were identified on WC and Pd/WC using high-resolution electron energy loss spectroscopy (HREELS) in a separate UHV chamber (base pressure 2 × $10^{-10}$ Torr) equipped with AES and HREELS. The HREELS results were acquired with a primary beam energy of 6 eV. The angles of incidence and reflection were 60° with respect to the surface normal. Count rates in the elastic peak were typically between 1 × $10^4$ and 3 × $10^4$ counts per second, and the spectral resolution was between 30 and 50 $cm^{-1}$ full width at half-maximum (fwhm). Each HREEL spectrum was normalized to unity using the elastic peak intensity and then scaled by a multiplication factor.

*2.2.2. Electrochemical Measurements.* The WC electrodes were prepared using the same polycrystalline W foil as in the UHV studies. The W foil was first rinsed with methanol and deionized water and was then dipped in 0.3 M NaOH to remove surface oxides. The samples were dried and heated in a Lindberg furnace (Model 55035) in the presence of methane ($CH_4$) and hydrogen ($H_2$) up to 1000 °C and held there for 1 h to produce a WC thin film. The flow rates of $CH_4$ and $H_2$ were 33 and 122 sccm, respectively. As the temperature was decreasing the $CH_4$ flow was turned off at 875 °C, with the rest of the ramp down in temperature under $H_2$ gas flow to obtain a WC film free of excess surface carbon.[31] After the samples reached room temperature they were passivated by flowing a 1% $O_2$ and 99% $N_2$ gas mixture over the surface for 3 h. This passivation procedure minimized the further oxidation of WC in air during sample transfer to the electrochemical cell or the Pd deposition chamber. The WC surfaces were then characterized using XPS to determine the atomic W/C ratio. The peak intensities were normalized by the XPS sensitivity factors[32] to confirm the 1:1 ratio of carbidic carbon to metallic tungsten ratio.

The Pd-modified WC electrodes were synthesized in a vacuum system equipped with a Pd evaporative deposition source. The samples were then transferred to a vacuum system with X-ray photoelectron spectroscopy (XPS) to determine the Pd coverage.

Similar to previous XPS and AES studies of the growth mechanism of Ni[33] and Pt[33,34] on the WC substrate, XPS measurements were performed as a function of Pd deposition time at 300 K, as shown in Figure 2. As described in the previous studies,[33,34] the growth of Ni and Pt on WC followed the layer-by-layer growth mechanism, with the completion of the first monolayer being indicated by a break in the slope of the Ni and Pt uptake curve. The Pd uptake curve in Figure 2


dx.doi.org/10.1021/cs200620x | ACS Catal. 2012, 2, 751–758

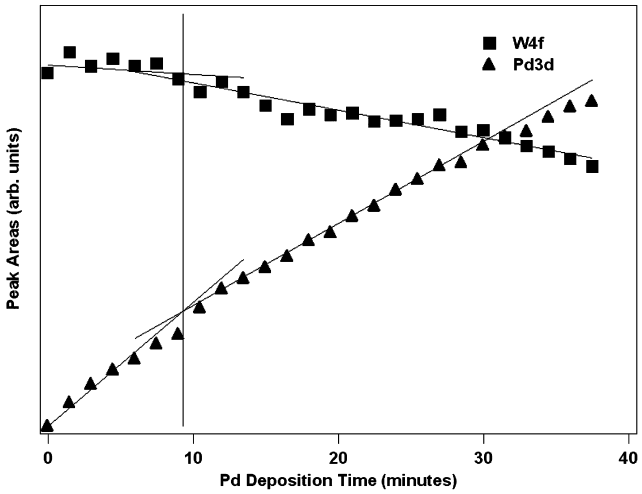


**Figure 2.** XPS measurements taken during thermal evaporation of Pd onto a WC foil. Change in Pd3d and W4f peak areas as a function of deposition time.

shows a break at the deposition time of approximately 9 min, with a similar break also observed in the W signal. Using the XPS sensitivity factors and overlayer calculations, the Pd/W XPS ratio at 9 min also corresponds to the completion of the first monolayer. The results in Figure 2 suggest that, similar to Ni and Pt, the deposition of Pd on WC also leads to a layer-by-layer growth mechanism.

The WC, Pd/WC, and Pd electrodes were mounted in a three-electrode cell with a static 400 mL volume of 0.01 M KOH (Fisher Scientific) electrolyte. The cell was deaerated with $N_2$ via a sparger. A saturated calomel reference electrode (SCE) and a Pt mesh counter electrode were used in the cell. The current responses shown in each voltammetry study were normalized to the surface area of the working electrode. A Princeton Applied Research VersaSTAT 4 Potentiostat/Galvanostat was used for cyclic voltammetry (CV) and chronoamperometry (CA) measurements. All potentials are reported versus the normal hydrogen electrode (NHE).

## 3. RESULTS AND DISCUSSION

**3.1. DFT Calculations of Binding Energies of Methanol and Methoxy.** The binding energies of methanol and methoxy are summarized in Table 1. On every surface, methanol adsorbed in the atop site, but methoxy was able to bind in four different sites. This behavior has been previously observed and is attributed to repulsive interactions between the hydroxyl group and the surface.[24] The structure of methanol was not perturbed by adsorption; in addition, the metal−oxygen bond length did not differ by more than 0.05 Å between the surfaces. Methoxy was most stable in the highly coordinated sites. The C−O bond of methoxy lengthened upon adsorption. Comparing to the gas phase value of 1.36 Å, the C−O bond length was 1.44 Å on Pd(111) and Pd/WC, and 1.48 Å on WC. The greater length on WC compared to the other surfaces suggests a weakening of the bond, which is consistent with the observed selectivity of C−O bond scission to produce methane, as described later. The distance in the *z*-dimension between the surface plane and methoxy also varied, following the trend WC < Pd(111) < Pd/WC. The low distance in the case of WC makes all bonds accessible to the surface, contributing to the pathway for total decomposition. The trend in the binding energy is consistent with that calculated in previous studies of adsorbates on WC and metal-modified WC surfaces.[24,35] For both methanol and methoxy, WC shows the highest binding energy, and adding a monolayer of Pd decreases the binding energy closer to that of Pd(111). The methanol and methoxy binding energies on Pd(111) are in general agreement with the literature.[36−39] The trend in Table 1 predicts that Pd-modified WC surfaces should show activity more similar to Pd(111) than to WC. Additionally, Pd/WC should show higher total activity than Pd(111) because of its higher adsorbate binding energy.

**Table 1. Binding Energies of Methanol and Methoxy on WC, Pd/WC, and Pd(111)**

| | BE (kcal/mol) | | | | |
|---|---|---|---|---|---|
| | | methoxy | | | |
| surface | methanol | binding site | | | |
| | atop | atop | fcc | hcp | bridge |
| WC | −15.86 | −66.38 | −81.94 | −91.09 | −73.95 |
| Pd/WC | −8.58 | −48.62 | −55.33 | −54.84 | −52.25 |
| Pd(111) | −5.56 | −33.79 | −38.00 | −37.69 | −37.22 |

**3.2. TPD of Methanol on WC, Pd/WC, and Pd(111).** TPD experiments were performed to determine the activity and selectivity of methanol decomposition on WC, Pd-modified WC, and Pd(111). The TPD spectra from 2 Langmuirs (1 $L = 1 \times 10^{-6}$ Torr-s) of methanol dosed at 100 K are shown in Figure 3. Multilayer methanol desorption was detected between 145 and 153 K from all the surfaces. Monolayer desorption of methanol occurred at 248 K from WC and 180 K from Pd/WC. The desorption of the $H_2$ product is shown in Figure 3b, with broad peaks centered at 398 K, 365 K, 335 and 296 K for WC, 0.5 ML Pd/WC, 1 ML Pd/WC, and Pd(111), respectively. Figure 3c shows the production of $CH_4$ at 410 K from WC and 0.5 ML Pd/WC, indicating that these two surfaces were also active toward breaking the C−O bond. This C−O bond breaking activity is removed by the higher loading of Pd on the surface. The desorption of the CO product (Figure 3d) occurred at approximately 392, 410, 431, and 469 K for WC, 0.5 ML Pd/WC, 1 ML Pd/WC, and Pd(111), respectively. The TPD results in Figure 3 suggest that adsorbed methanol can undergo decomposition via the following net reaction pathways:

$$a\mathrm{CH_3OH} \rightarrow a\mathrm{C_{ad}} + a\mathrm{O_{ad}} + 2a\mathrm{H_2}$$

(Complete Decomposition)

$$b\mathrm{CH_3OH} \rightarrow b\mathrm{CO} + 2b\mathrm{H_2}$$

(Reforming) (**Desired Reaction**)

$$c\mathrm{CH_3OH} \rightarrow c\mathrm{CH_4} + c\mathrm{O_{ad}}$$ (Methane Production)

where *a*, *b*, and *c* are the amount of adsorbed methanol decomposing from each given reaction pathway. The reforming reaction is desired because the selective O−H and C−H bond scission, with the C−O bond remaining intact, is similar to the initial steps in the electro-oxidation of methanol in DMFC. Quantification of the TPD results from WC and Pd/WC surfaces is summarized in Table 2. The quantification of methanol decomposition pathways on Pd(111) is from a previous study by Barteau and Davis.[40] The comparison in Table 2 reveals that the complete decomposition pathway is


dx.doi.org/10.1021/cs200620x | ACS Catal. 2012, 2, 751−758

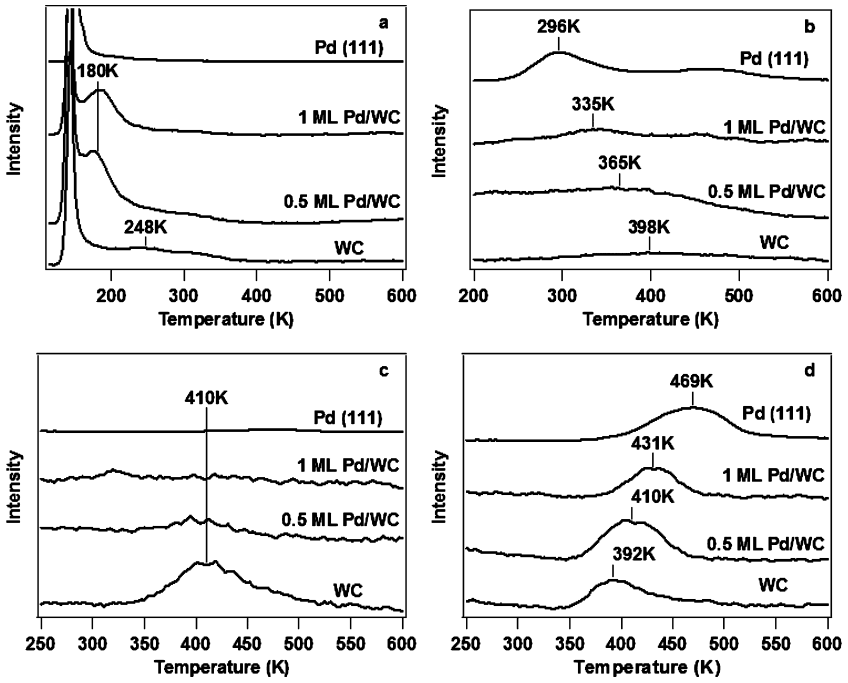


**Figure 3.** TPD spectra of (a) $CH_3OH$, (b) $H_2$, (c) $CH_4$, and (d) CO, following 2 L exposure of $CH_3OH$. The peak intensities from Pd(111) are not normalized to those from the WC and Pd/WC surfaces.

**Table 2. Activity of Methanol Decomposition on WC, Pd-Modified WC, and Pd(111) surfaces**

| | methanol activity (ML) | | | |
|---|---|---|---|---|
| surface | reforming | decomposition | $CH_4$ | total |
| WC | 0.020 | 0.182 | 0.023 | 0.225 |
| 0.5 ML Pd/WC | 0.183 | 0.083 | 0.011 | 0.277 |
| 1 ML Pd/WC | 0.053 | 0.152 | 0.000 | 0.205 |
| Pd (111) | 0.079[a] | 0.000[a] | 0 | 0.079[a] |

[a]Ref 40.

dominant for the WC surface, with the remaining products being from the reforming and methane production pathways. The methane production pathway is significantly reduced on the 0.5 ML Pd/WC surface and is absent on the 1 ML Pd/WC surface.

The TPD results following the adsorption of 4 L CO on WC, Pd/WC, and Pd(111) surfaces are shown in Figure 4. By comparing Figure 4 and Figure 3d, the desorption temperatures of CO from methanol decomposition were higher than those from molecularly adsorbed CO on the WC and Pd/WC surfaces, indicating a reaction-limited desorption for the CO product. In addition, molecularly adsorbed CO (Figure 4) desorbed from Pd/WC at lower temperatures than from Pd(111),[37] and Pd(110)[41] indicating that supporting Pd on WC weakened the binding energy of CO. The Redhead equation[42] was used to estimate the binding energies of CO to the surfaces. The binding energies for the CO peaks from WC were 17.2 and 21.3 kcal/mol while for the 0.5 ML Pd/WC, 1 ML Pd/WC, and Pd(111) surfaces the desorption peaks corresponded to binding energies of 19.3, 19.8, and 26.9 kcal/mol, respectively. The weaker CO binding energy on Pd/WC would potentially lead to a higher CO-tolerance on Pd/WC than on Pd, as discussed later.

**3.3. HREELS of Methanol on WC and Pd/WC.** Figure 5 shows the HREEL spectra of methanol on WC, 0.5 ML Pd/

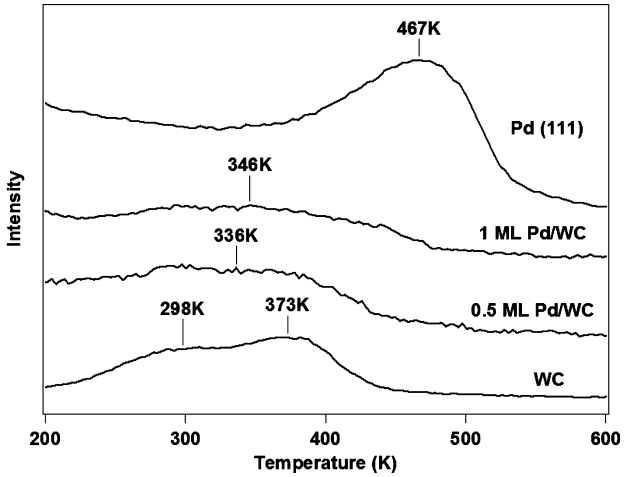


**Figure 4.** TPD spectra of CO following 4 L exposure of CO on WC, Pd/WC, and Pd(111) surfaces.

WC, and 1 ML Pd/WC surfaces. Methanol was dosed at 100 K, and the surface was then heated to temperatures between 200 and 500 K before cooling down to 100 K for HREELS measurements. Table 3 shows the vibrational assignments for adsorbed methanol on WC and Pd-modified WC. The HREEL spectra of methanol on WC showed that the O−H bond scission occurred even at 100 K, as suggested by the absence of the O−H stretching mode near 3300 $cm^{-1}$ and the deformation mode near 730 $cm^{-1}$. The resulting methoxy species remained on the surface up to 400 K. After heating to 500 K the C−O stretching and $CH_3$ rocking modes of methoxy disappeared, leaving only vibrational modes characteristic of surface $CH_x$ fragments. This is consistent with the TPD results (Figure 3) that showed $CH_4$ and CO desorbing from the surface between 400 and 500 K.

For the Pd-modified surfaces (Figure 5b and 5c), the spectroscopic changes were very different from those on WC.


dx.doi.org/10.1021/cs200620x | ACS Catal. 2012, 2, 751−758

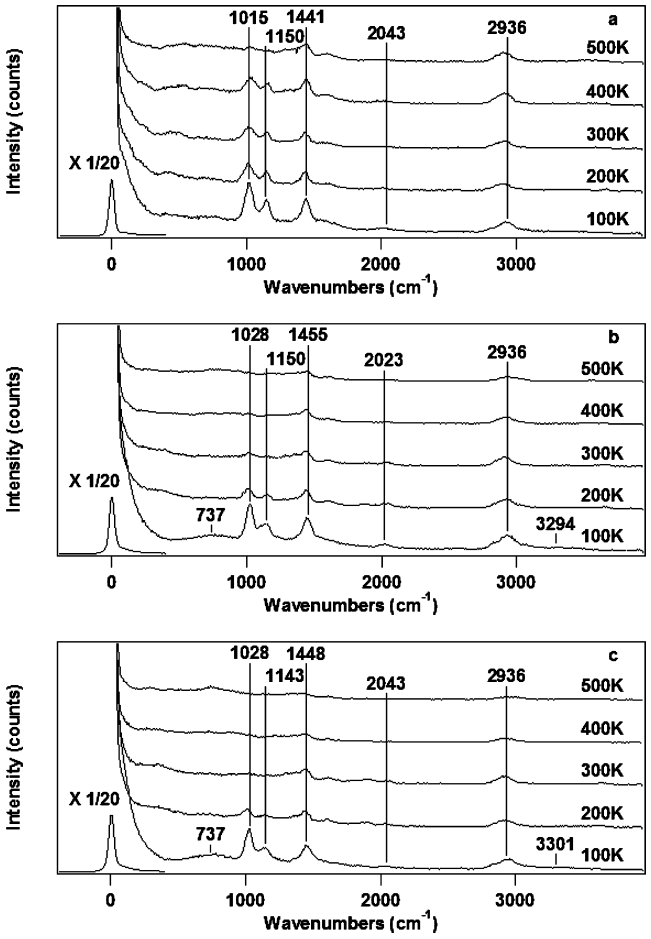


**Figure 5.** HREELS spectra of (a) WC, (b) 0.5 ML Pd/WC, and (c) 1 ML Pd/WC following 2 L exposure of $CH_3OH$.

**Table 3. HREELS Assignments for Methanol**[a]

| mode | gas-phase | liquid-phase | WC | Pd(111) | 1 ML Pd/WC |
|---|---|---|---|---|---|
| $\nu$(OH) | | | | | 3301 |
| $\nu$as($CH_3$) | 3000, 2960[c] | 2980, 2946[c] | 2936 | 3015, 2865[b] | 2936 |
| $\nu$(CO) | | | 2043 | 1805[b] | 2043 |
| $\delta$($CH_3$) | 1455, 1477[c] | 1480[c] | 1441 | 1430, 1375[b] | 1448 |
| $\rho$($CH_3$) | 1124[d] | | 1150 | 1140[b] | 1143 |
| $\nu$s(CO) | 1033[c] | 1030[c] | 1015 | 1005[b] | 1028 |
| $\delta$(OH) | | | | | 737 |

[a]Vibrational frequencies listed in $cm^{-1}$. [b]Ref 43. [c]Ref 44. [d]Ref 45.

At 100 K at least a fraction of methanol adsorbed with the O–H bond intact on the Pd-modified WC surfaces, as indicated by the presence of weak features at ~3301 $cm^{-1}$ and 737 $cm^{-1}$. The mixture of molecularly adsorbed methanol and methoxy is in agreement with what was observed by Davis and Barteau[43] on Pd(111), although on Pd(111) methanol is found to react to form CO and $H_2$ through a $\eta^2$-formaldehyde. The 200 K spectra were characteristic of methoxy formation on the Pd/WC surfaces, without the characteristic $\eta^2$-formaldehyde features.[43] The C–O stretching and $CH_3$ rocking modes, at 1028 and 1143 $cm^{-1}$, respectively, decreased upon heating to 300 K on the 0.5 ML Pd/WC surface and completely disappeared above 300 K. The characteristic methoxy vibrational features disappeared at 300 K on the 1 ML Pd/WC surfaces. There was also no indication that there was adsorbed CO on the surfaces above 300 K. The HREELS results in Figure 5 indicated that the presence of Pd on WC significantly decreased the dissociation temperature of methoxy. Comparing to previous studies, the decomposition temperature of surface methoxy on Pd/WC was lower than the reaction temperature on Pt/WC,[35] Au/WC,[24] Ni/WC[24] and was similar to Rh/WC.[24]

Overall, the TPD (Figure 3) and HREELS (Figure 5) results indicate that pure WC would not be an effective DMFC electrocatalyst because of its activity toward the C–O bond scission to produce $CH_4$. In contrast, the presence of Pd on WC enhances the C–H bond scission, leading to the decomposition of surface methoxy at lower temperatures and the formation of the desirable products of CO and $H_2$. These UHV surface science results predict that Pd-modified WC should be a promising electrocatalysts for DMFC. Furthermore, on the basis of the summary in Table 2, the 1 ML Pd/WC surface shows the absence of $CH_4$ formation while maintaining a relatively high activity toward CO and $H_2$ production. For this reason the 1 ML Pd/WC surface was selected for electrochemical evaluation to verify the UHV surface science prediction.

**3.4. Electrochemical Evaluation of Methanol Electro-oxidation on WC, Pd/WC, and Pd.** Figure 6 compares the cyclic voltammetry (CV) results of foil samples of WC, 1 ML Pd/WC, and Pd. The samples were cycled between 0.05 and 1.05 V in a solution of 0.01 M KOH and 2 M $CH_3OH$. As shown in Figure 6a, a relatively weak oxidation peak was observed at 0.74 V on WC. The Pd modification of WC resulted in an increase in the activity for the electro-oxidation of methanol. The 1 ML Pd/WC surface (Figure 6b) showed methanol oxidation on the forward scan starting at 0.60 V with a peak at 0.89 V and on the reverse scan beginning at 0.80 V with a peak at 0.71 V. The Pd sample (Figure 6c) showed methanol oxidation on the forward scan starting at 0.60 V with a peak at 0.86 V and on the reverse scan beginning at 0.90 V with a peak at 0.77 V. The intensity ratios of the anodic (forward) to the cathodic (backward) peak current (If/Ib) for the 1 ML Pd/WC and Pd foils were analyzed. The If/Ib ratio was 1.78 and 3.18 for the 1 ML Pd/WC and Pd foils, respectively. As reported by Manoharan et al. and others,[46–51] the higher the If/Ib ratio the more improved CO tolerance and catalytic activity. However, a new study by Hofstead-Duffy et al.[52] observes that both forward and reverse peaks were from methanol oxidation, and that a better measure for CO tolerance would be the steady-state oxidation current.

To compare the steady-state oxidation current, Figure 7 shows the chronoamperometry (CA) results of methanol oxidation on 1 ML Pd/WC and Pd. The CA scans were performed for 2 h at 0.85 V in a 0.01 M KOH and 2 M $CH_3OH$ solution. The 1 ML Pd/WC foil maintained a higher steady-state current density than the Pd foil. This was possibly due to an enhanced CO tolerance on Pd/WC, as suggested from the TPD results (Figures 3 and 4), with CO desorbing at lower temperatures from 1 ML Pd/WC than from Pd(111). This is similar to what was reported by Stottlemyer and Weigert for 0.8 ML Pt/WC in comparison to Pt foil in an acidic electrochemical environment.[53]

**3.5. Stability of WC and 1 ML Pd/WC in Electrochemical Environment.** Figure 8 compares the XPS spectra of WC foil recorded before and after the CA measurements at


dx.doi.org/10.1021/cs200620x | ACS Catal. 2012, 2, 751–758

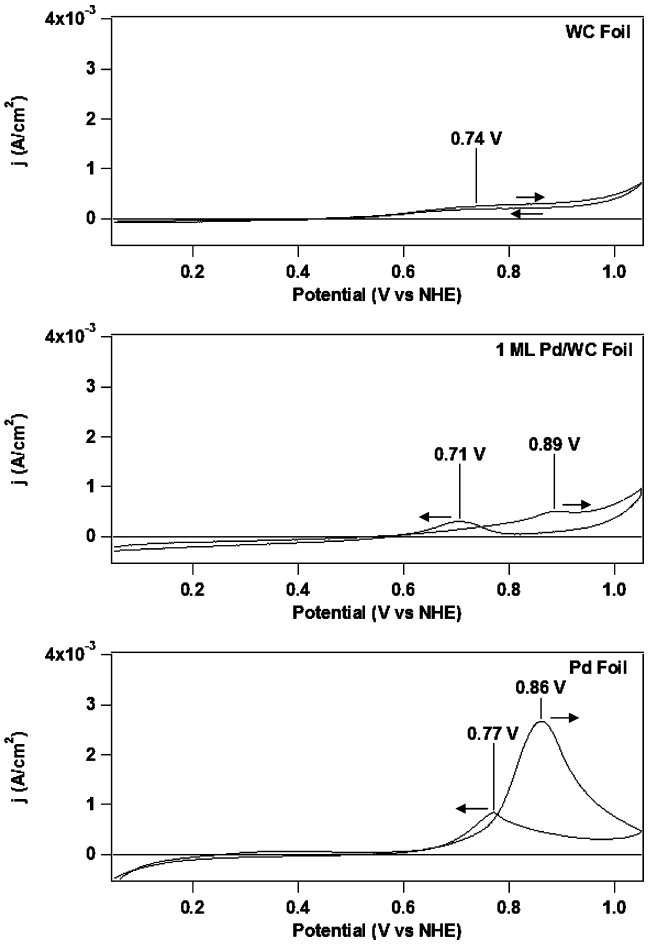


**Figure 6.** Cyclic voltammetry in 2 M $CH_3OH$ and 0.01 M KOH of (a) WC foil, (b) 1 ML Pd/WC foil, and (c) Pd foil. The CV curves were the 100th scan for each sample.

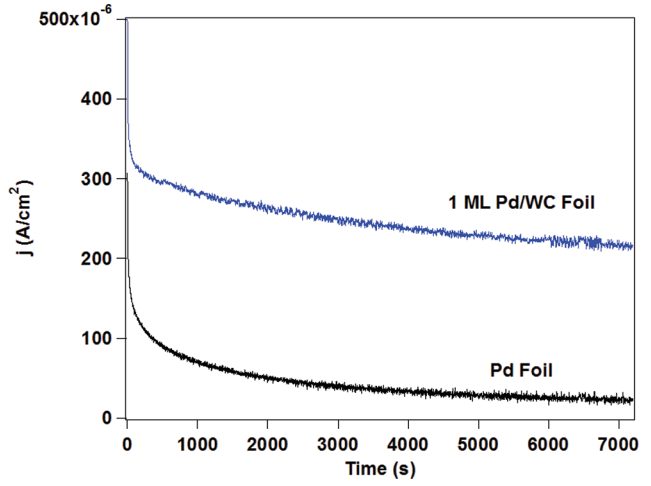


**Figure 7.** Chronoamperometry of 1 ML Pd/WC foil and Pd foil at 0.85 V vs NHE in 2 M MeOH and 0.01 M KOH.

the potential of 0.85 V. As shown in Figure 8a, the W 4f peaks for WC were observed at 31.3 and 33.2 eV. The near absence of tungsten oxide peaks, expected at approximately 36 and 38 eV,[14] confirmed that the WC surface was not significantly oxidized during the 2 h CA measurements. The C 1s peaks in Figure 8b showed a carbonaceous carbon feature at 284.4 eV

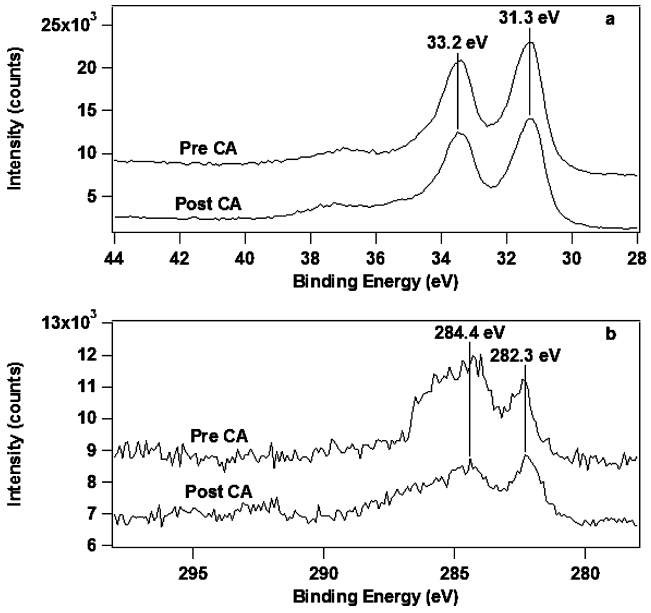


**Figure 8.** XPS spectra of WC foil before and after 2 h CA measurements for (a) W 4f region, and (b) C 1s region.

and a carbidic carbon feature at 282.3 eV.[32] The ratio of XPS peaks of tungsten to carbidic carbon was similar for the pre- and post-CA samples, suggesting that the WC stoichiometry was not altered during the electrochemical measurements.

The absence of oxidized tungsten in the post-CA XPS spectrum suggested that the WC film remained stable during the electrochemical measurements. Although one could not rule out the possibility that some of the WC surfaces were oxidized and the $WO_x$ species were subsequently dissolved into the solution, such oxidation/dissolution would convert some of the carbidic carbon into carbonaceous carbon. This hypothesis was inconsistent with the XPS measurements, which showed that the carbonaceous carbon in the post-CA spectrum was slightly reduced as compared to the pre-CA spectrum.

Figure 9 compares the XPS spectra of 1 ML Pd/WC foil recorded before and after the CA measurements at the potential of 0.85 V. As shown in Figure 9a, the Pd 3d peaks at 335.2 and 340.8 eV decrease by approximately 20% after the 2 h CA experiment, which could be attributed to either Pd dissolution or agglomeration. Similar to those observed for unmodified WC, the CA experiment did not noticeably change the intensities of the W4f and carbidic carbon peaks of the 1 ML Pd/WC surface.

## 4. DISCUSSION

A comparison of the DFT calculations (Table 1) and the TPD quantification (Table 2) show a correlation between the binding energy of methoxy and the reaction pathways of methanol on WC, Pd/WC, and Pd(111). The HREELS results in Figure 5 confirm the presence of methoxy as the surface intermediate from the decomposition of methanol on WC and Pd/WC surfaces.

On the unmodified WC surface, DFT calculations predict that methoxy bonds to the surface very strongly through the oxygen atom, with a significantly lengthened C−O bond comparing to the gas-phase values. Such strong weakening of the C−O bond leads to its cleavage to produce the $CH_3$ fragment that recombines with atomic hydrogen and desorbs as


dx.doi.org/10.1021/cs200620x | ACS Catal. 2012, 2, 751−758

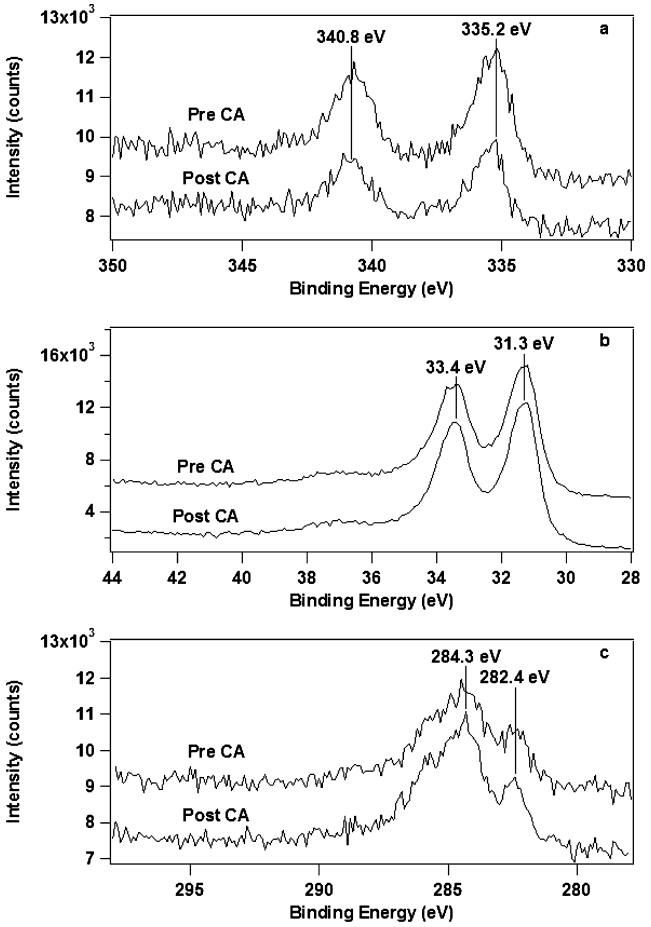


**Figure 9.** XPS spectra 1 ML Pd/WC foil before and after 2 h CA measurements for (a) Pd 3d region, (b) W 4f region, and (c) C 1s region.

$CH_4$, as verified in the TPD measurements. The binding energy of methoxy is substantially reduced upon the deposition of submonolayer and monolayer of Pd on WC, eliminating the $CH_4$ reaction pathway from Pd/WC. Furthermore, comparing to Pd(111), the stronger binding energy of methoxy on Pd/WC should lead to a higher extent of methanol reaction, as confirmed in the TPD results in Table 2.

The TPD results in Table 2 suggest that, similar to Pd, the Pd/WC surfaces should be active for methanol electro-oxidation. Equally important, the TPD results following the desorption of CO (Figure 4) reveals that CO bonds more weakly on Pd/WC than on Pd(111), demonstrating the potential of using Pd/WC as a more CO-tolerant electrocatalyst. Such predictions from DFT calculations and UHV surface science studies are confirmed in the corresponding CA experiments. The higher activity and stability of Pd/WC in the steady-state measurement in Figure 7 is consistent with Pd/WC being more CO-tolerant than Pd foil.

Finally, in the current study well-characterized thin films of WC and Pd/WC are used as model systems to demonstrate the correlation between DFT calculations, UHV measurements, and electrochemical evaluation. For practical applications porous powder Pd/WC catalysts will need to be synthesized and evaluated for fuel cell applications. In our previous studies of Pt/WC electrocatalysts, results from the thin film model surfaces have been extended to powder Pt/WC catalysts for both methanol oxidation[53] and hydrogen evolution[54] reactions. Similar synthesis and electrochemical evaluation of powder Pd/WC catalysts should be explored to extend the promising properties described in the current study to practical electrochemical applications.

## 5. CONCLUSIONS

The current study combines DFT calculations and UHV surface science studies to compare the reaction pathways of methanol on WC, Pd/WC, and Pd surfaces and to evaluate the feasibility of using Pd/WC as electrocatalysts in DMFC. DFT calculations reveal that the binding energies of methanol and methoxy on the 1 ML Pd/WC surface are similar to those on Pd(111). This is supported by the HREELS results that methoxy reacts on the Pd/WC surface to produce CO and $H_2$, similarly to Pd(111).[43] Furthermore, TPD results reveal that the desorption temperatures of CO from Pd/WC are lower than that from Pd(111), suggesting a potentially higher CO tolerance on the Pd/WC surfaces. These DFT and UHV predictions are verified using electrochemical measurements, which show that the 1 ML Pd/WC surface is active for the electro-oxidation of methanol. Steady-state CA measurements at 0.85 V also show that Pd/WC is more active than Pd, likely because of the higher CO tolerance of Pd/WC. XPS measurements before and after the 2 h CA measurements demonstrate promising results regarding the stability of Pd/WC in the alkaline environment. Further studies on the stability of Pd/WC, in both half-cell and full-cell measurements, are needed to further evaluate the potential utilization of Pd/WC, with Pd coverage in the monolayer range, as the lower-cost anode catalysts for DMFC.

## AUTHOR INFORMATION

### Corresponding Author

*E-mail: jgchen@udel.edu.

### Funding

This work was supported by the Department of Energy, Office of Basic Energy Sciences (DOE/BES Grant DE-FG02-00ER15104).

### Notes

The authors declare no competing financial interest.

## REFERENCES

(1) Lamy, C.; Belgsir, E. M.; Leger, J.-M. *J. Appl. Electrochem.* **2001**, *31*, 799.
(2) Peled, E.; Duvdevani, T.; Aharon, A.; Melman, A. *Electrochem. Solid-State Lett.* **2001**, *4*, A38.
(3) Liu, H.; Song, C.; Zhang, L.; Zhang, J.; Wang, H.; Wilkinson, D. P. *J. Power Sources* **2006**, *155*, 95−110.
(4) Deluca, N. W.; Elabd, Y. A. *J. Polym. Sci., Part B: Polym. Phys.* **2006**, *44*, 2201−2225.
(5) Shukla, A. K.; Raman, R. K. *Annu. Rev. Mater. Res.* **2003**, *33*, 155−168.
(6) Park, K.-W.; Sung, Y.-E.; Han, S.; Yun, Y.; Hyeon, T. *J. Phys. Chem. B* **2004**, *108*, 939−944.
(7) Noto, V. D.; Negro, E.; Gliubizzi, R.; Lavina, S.; Pace, G.; Gross, S.; Maccato, C. *Adv. Funct. Mater.* **2007**, *17*, 3626−3638.
(8) Antolini, E. *Energy Environ. Sci.* **2009**, *2*, 915−931.
(9) Koczkur, K.; Li, Q.; Chen, A. *Adv. Mater.* **2007**, *19*, 2648−2652.
(10) Zhao, Y.; Fan, L.; Zhong, H.; Li, Y.; Yang, S. *Adv. Funct. Mater.* **2007**, *17*, 1537−1541.
(11) Liu, B.; Li, H. Y.; Die, L.; Zhang, X. H.; Fan, Z.; Chen, J. H. *J. Power Sources* **2009**, *186*, 62−66.
(12) Singh, R. N.; Singh, A.; Anindita. *J. Hydrogen Energy* **2009**, *34*, 2052−2057.

(13) Ha, S.; Larsen, R.; Masel, R. I. *J. Power Sources* **2005**, *144*, 28−34.
(14) Esposito, D. V.; Chen, J. G. *Energy Environ. Sci.* **2011**, *4*, 3900−3912.
(15) Hwu, H. H.; Chen, J. G. *Chem. Rev.* **2005**, *105*, 185−212.
(16) Venkataraman, R.; Kunz, H. R.; Fenton, J. M. *J. Electrochem. Soc.* **2003**, *150*, A278−A284.
(17) Mellinger, Z. J.; Weigert, E. C.; Stottlemyer, A. L.; Chen, J. G. *Electrochem. Solid-State Lett.* **2008**, *11*, B63−B67.
(18) Hu, F. P.; Shen, P. K. *J. Power Sources* **2007**, *173*, 877−881.
(19) Zellner, M. B.; Chen, J. G. *Catal. Today* **2005**, *99*, 299−307.
(20) Lee, Y.-W.; Ko, A.-R.; Han, S.-B.; Kim, H.-S.; Kim, D.-Y.; Kim, S.-J.; Park, K.-W. *Chem. Commun.* **2010**, *46*, 9241−9243.
(21) Kresse, G.; Hafner, J. *J. Phys. Rev. B* **1993**, *47*, 558.
(22) Kresse, G.; Furthmuller, J. *J. Comput. Mater. Sci.* **1996**, *6*, 15.
(23) Kresse, G.; Furthmuller, J. *J. Phys. Rev. B* **1996**, *54*, 11169.
(24) Kelly, T. G.; Stottlemyer, A. L.; Ren, H.; Chen, J. G. *J. Phys. Chem. C* **2011**, *115*, 6644.
(25) Weigert, E. C.; Zellner, M. B.; Stottlemyer, A. L.; Chen, J. G. *Top. Catal.* **2007**, *46*, 349−357.
(26) Davis, L. E.; MacDonald, N. C.; Palmberg, P. W.; Riach, G. E.; Weber, R. E. *Handbook of Auger Electron Spectroscopy*; Physical Electronics Industries, Inc.: Eden Prairie, MN, 1976.
(27) Weigert, E. C.; Esposito, D. V.; Chen, J. G. *J. Power Sources* **2009**, *193*, 501−506.
(28) Childs, K. D.; Carlson, B. A.; LaVanier, L. A.; Moulder, J. F.; Paul, D. F.; Stickle, W. F.; Watson, D. G. *Handbook of Auger Electron Spectroscopy*, 3rd ed.; Physical Electronics, Inc.: Eden Prairie, MN, 1995; p 405.
(29) Cumpson, P. J.; Seah, M. P. *Surf. Interface Anal.* **1997**, *25*, 430−446.
(30) Stottlemyer, A. L.; Ren, H.; Chen, J. G. *Surf. Sci.* **2009**, *603*, 2630−2638.
(31) Kimmel, Y. C.; Esposito, D. V.; Birkmire, R. W.; Chen, J. G. *J. Hydrogen Energy* **2012**, *37*, 3019−3024.
(32) Moulder, J. F.; Stickle, W. F.; Sobol, P. E.; Bomben, K. D. *Handbook of X-ray Photoelectron Spectroscopy*; Physical Electronics, Inc.: Eden Prairie, MN, 1995.
(33) Humbert, M. P.; Menning, C. A.; Chen, J. G. *J. Catal.* **2010**, *271*, 132−139.
(34) Esposito, D. V.; Hunt, S. T.; Stottlemyer, A. L.; Dobson, K. D.; McCandless, B. E.; Birkmire, R. W.; Chen, J. G. *Angew. Chem., Int. Ed.* **2010**, *49*, 9859−9862.
(35) Stottlemyer, A. L.; Liu, P.; Chen, J. G. *J. Chem. Phys.* **2010**, *133*, 104702.
(36) Jiang, R. B.; Guo, W. Y.; Li, M.; Fu, D. L.; Shan, H. H. *J. Phys. Chem. C* **2009**, *113*, 4188.
(37) Schennach, R.; Eichler, A.; Rendulic, K. D. *J. Phys. Chem. B* **2003**, *107*, 2552.
(38) Zhang, C. J.; Hu, P. *J. Chem. Phys.* **2001**, *115*, 7182.
(39) Chen, Z.-X.; Neyman, K. M.; Lim, K. H.; Rösch, N. *Langmuir* **2004**, 20.
(40) Davis, J. L.; Barteau, M. A. *Surf. Sci.* **1987**, *187*, 387−406.
(41) Shekhar, R.; Barteau, M. A. *Catal. Lett.* **1995**, *31*, 221−237.
(42) Redhead, P. A. *Vacuum* **1962**, *12*, 203−211.
(43) Davis, J. L.; Barteau, M. A. *Surf. Sci.* **1990**, *235*, 235−248.
(44) Skoplyak, O.; Menning, C. A.; Barteau, M. A.; Chen, J. G. *J. Chem. Phys.* **2007**, *127*, 114707.
(45) Falk, M.; Whalley, E. *J. Chem. Phys.* **1961**, *34*, 1554.
(46) Manoharan, R.; Goodenough, J. B. *J. Mater. Chem.* **1992**, *2*, 875−887.
(47) Kang, W.-D.; Wei, Y.-C.; Liu, C.-W.; Wang, K.-W. *Electrochem. Commun.* **2011**, *13*, 162−165.
(48) Yen, C. H.; Shimizu, K.; Lin, Y.-Y.; Bailey, F.; Cheng, I. F.; Wai, C. M. *Energy Fuels* **2007**, *21*, 2268−2271.
(49) Yin, M.; Huang, Y.; Liang, L.; Liao, J.; Liu, C.; Xing, W. *Chem. Commun.* **2011**, *47*, 8172−8174.
(50) Yoo, E.; Okata, T.; Akita, T.; Kohyama, M.; Nakamura, J.; Honma, I. *Nano Lett.* **2009**, *9*, 2255−2259.
(51) Zhang, L. J.; Wang, Z. Y.; Xia, D. G. *J. Alloys Compd.* **2006**, *426*, 268−271.
(52) Hofstead-Duffy, A. M.; Chen, D.-J.; Sun, S.-G.; Tong, Y. J. *J. Mater. Chem.* **2012**, *22*, 5205−5208.
(53) Stottlemyer, A. L.; Weigert, E. C.; Chen, J. G. *Ind. Eng. Chem. Res.* **2011**, *50*, 16−22.
(54) Hsu, I. J.; Kimmel, Y. C.; Jiang, X. J.; Willis, B. G.; Chen, J. G. *Chem. Commun.* **2012**, *48*, 1063−1065.